Hyperfine structures of Ca^+ and Sr^+ ions: Summary of trends in hyperfine interactions in the alkaline-earth-metal ions and corresponding series with similar electronic structures

Xing Yuan, S. N. Panigrahy,* R. W. Dougherty,† and T. P. Das
Department of Physics, State University of New York at Albany, Albany, New York 12222

J. Andriessen
Technische Natuurkunde, Technische Universiteit Delft, 2628 CJ Delft, The Netherlands
(Received 22 December 1994)

The hyperfine interactions in the alkaline-earth-metal ions, Ca^+ and Sr^+, have been investigated using the relativistic linked-cluster many-body perturbation theory (RLCMBPT). The calculated theoretical hyperfine fields are found to be 135.3 and 266.3 T for Ca^+ and Sr^+, respectively, in good agreement with the experimentally obtained values of 139.0 T for Ca^+ and 267.2 T for Sr^+. The contributions from the various mechanisms, direct, exchange core polarization, and many-body correlation effects, are analyzed and combined with results obtained from earlier first-principles RLCMBPT investigations to study the trends in the relative importance of these mechanisms over the entire alkaline-earth-metal series. These trends are compared to the corresponding ones found for other single *s*-valence electron series, namely, the alkali-metal-atom, noble-metal-atom, and group-IIB-ion series. A number of similar features involving the behaviors of the exchange core polarization and correlation effects within and among these series are observed. Several factors, such as the deformabilities of the valence electron shells, the relative separations between core and valence electrons, and the effective charges of the systems, are analyzed to achieve a satisfactory general understanding of the physical underlining of the observed features in these trends.

PACS number(s): 31.30.Gs, 31.25.−v, 31.30.Jv, 32.10.−f

I. INTRODUCTION

The relativistic linked-cluster many-body perturbation theory (RLCMBPT) [1] method has been used successfully in the investigation of hyperfine properties of a number of atomic systems [2]. The present work is concerned with the ground states of $^{43}Ca^+$ and $^{87}Sr^+$ ions. There is a number of reasons why the investigation of these ions is important at the present time. The first reason is that the experimental hyperfine constants for these two systems have been available for some time [3,4], making the results of completely first-principles theoretical studies on them accountable. Second, one can combine the results of the first-principles investigations on these two ions with corresponding ones already available in other ions [5] of the alkaline-earth-metal series to study the trends of the various contributions [1,2], namely, the direct contribution from the *s*-valence electron, the exchange core polarization (ECP) contributions from the core electrons, and many-body correlation effects. While these trends cannot at the present time be measured experimentally, the satisfactory nature of the agreement between the total hyperfine constants from theory and experiment provides indirect support for the theoretical results for these trends. The latter provide valuable insights [6] into the understanding of the mechanisms contributing to the corresponding physical effects. It is particularly interesting at the present time to study these trends for the added reason that similar trends are already available from first-principles RLCMBPT investigations in the three other related series with a single *s*-valence electron outside closed shells involving a neutral atom or singly charged positive ion, namely, the alkali-metal atoms [6], noble-metal atoms [7], and the corresponding isoelectronic singly charged Zn^+, Cd^+, and Ag^+ ions [8]. Finally, the understanding of the mechanisms contributing to the hyperfine fields at the nuclei of Ca^+ and Sr^+ ions is important because these ions occur as impurities in the high-T_c systems such as $YBa_2Cu_3O_7$ and La_2CuO_4. Since effects related to the hyperfine fields at Ca^+ and Sr^+ ions in high-T_c systems are experimentally measurable and a theoretical analysis in these complicated systems at the same level of accuracy as in free ions is difficult to achieve, results for the free-ion case provide useful insights into the solid-state systems.

Section II of this paper will discuss a few theoretical and computational aspects of the RLCMBPT procedure particularly pertinent to the present systems. Details of the procedure are available [1,2] in the literature. In Sec. III we shall discuss the results for the hyperfine fields in Ca^+ and Sr^+ and make comparisons to experiment and other available theoretical results. Section IV will deal with the trends in the direct, ECP, and correlation contributions in the alkaline-earth series and make comparisons

*Present address: Biology Divison, Argonne National Laboratory, Argonne, IL 60439.

†Present address: Condensed Matter Radiation Division, Naval Research Laboratory, Washington, DC 20375.

 ©1995 The American Physical Society

with the related series. Section V will present some concluding remarks.

II. PROCEDURE

The principles of the RLCMBPT procedure as applied to atomic systems have been described in detail in earlier literature [1,2]. We will, however, present some highlights of the theory here both for the sake of completeness and to facilitate the discussion of the results in Sec. III.

For an atomic system with a nuclear charge ζ and N electrons, the relativistic Hamiltonian is given by [9]

$$H=\sum_{i=1}^{N}(c\boldsymbol{\alpha}_i\cdot\mathbf{p}_i+\beta_i mc^2)-\sum_{i=1}^{N}\frac{\zeta e^2}{r_i}+\sum_{i>j}\frac{e^2}{r_{ij}}\ , \tag{1}$$

where e and m represent the electronic charge and the mass, α_i and β_i are the Dirac matrices for the ith electron, $\mathbf{r}_i$ represents its position vector with respect to the nucleus, $\mathbf{p}_i$ is its momentum vector, and r_{ij} is the distance between the ith and the jth electrons. For a relativistic treatment of magnetic hyperfine properties, one has to work with the relativistic hyperfine interaction Hamiltonian [1(c)]

$$H'_{\rm hyp}=ec\sum_i\boldsymbol{\alpha}_i\cdot\frac{\boldsymbol{\mu}_I\times\mathbf{r}_i}{r_i^3}\ , \tag{2}$$

in which $\boldsymbol{\mu}_I$ is the nuclear magnetic moment vector of the atomic system under study. For evaluating the hyperfine properties rigorously, one needs a knowledge of the exact many-electron eigenfunction Ψ_0 of the Hamiltonian H described in Eq. (1), satisfying the Dirac equation

$$H\Psi_0=E\Psi_0\ . \tag{3}$$

Because of the interactions between the electrons represented by the last term in Eq. (1), it is not possible to obtain Ψ_0 by directly solving Eq. (3). One therefore has to use approximation methods. In the RLCMBPT approach, we use a perturbation procedure in which the zeroth-order approximation to the Hamiltonian H in Eq. (1) is taken to be

$$H_0=\sum_{i=1}^{N}(c\boldsymbol{\alpha}_i\cdot\mathbf{p}_i+\beta_i mc^2)-\sum_i\frac{\zeta e^2}{r_i}+\sum_i V(r_i)\ , \tag{4}$$

where $V(r_i)$ is the one-electron V^{N-1} potential defined through its matrix elements by the relation

$$\langle a|V^{N-1}|b\rangle=\sum_{n=1}^{N-1}\left[\left\langle an\left|\frac{e^2}{r_{12}}\right|bn\right\rangle-\left\langle an\left|\frac{e^2}{r_{12}}\right|nb\right\rangle\right]\ , \tag{5}$$

in which n refers to the occupied states of the system, the summation in Eq. (5) being carried out over all but the outermost occupied, or valence, state in the present case. The reason that the V^{N-1} potential is chosen instead of the Hartree-Fock potential V^N is that the former is physically more meaningful [1(c)] for the excited states, since an electron in an excited state spends much of its time at a large distance away from the nucleus, where for a positive-ion system such as Ca^+ or Sr^+, it experiences effectively a potential due to a double positive charge at the nucleus. The V^{N-1} potential leads to such an effective potential at large distances, while the V^N potential leads to one corresponding to a single positive charge. It is therefore necessary to use the V^{N-1} potential for the excited states.

In principle, one should work with the complete set of occupied and excited states based on the V^{N-1} potential. However, certain additional diagrams would then occur that provide corrections that arise from the fact that the actual occupied states are eigenfunctions of the Hartree-Fock V^N potential. It has therefore been the practice in LCMBPT investigations, both relativistic and nonrelativistic, as discussed in earlier literature [10], to use occupied states generated in the Hartree-Fock V^N potential [with summation over n taken up to N rather than $N-1$ in Eq. (5)] and excited states from the V^{N-1} potential.

The Hamiltonian H_0 along with its eigenfunction Φ_0 now satisfies the equation

$$H_0\Phi_0=E_0\Phi_0\ , \tag{6}$$

which can be solved directly by well-established numerical procedures. The difference between the Hamiltonians H and H_0 of Eqs. (1) and (4) is considered as the perturbation Hamiltonian H' in RLCMBPT method, namely,

$$H'=H-H_0=\sum_{i>j}\frac{e^2}{r_{ij}}-\sum_i V_i^{N-1}\ . \tag{7}$$

The exact many-electron wave function Ψ_0 in Eq. (3) can be expressed by the linked-cluster expansion [11] in terms of Φ_0 in Eq. (6) in the form of

$$\Psi_0=\sum_{n=0}^{\infty}\left[\frac{H'}{E_0-H_0}\right]^n\Phi_0\ . \tag{8}$$

The expectation value of the hyperfine interaction Hamiltonian $H'_{\rm hyp}$ in Eq. (2) over Ψ_0 can now be written as [1(c)]

$$\langle\Psi_0|H'_{\rm hyp}|\Psi_0\rangle=\sum_{m,n}^{(L)}\left\langle\Phi_0\left|\left[\frac{H'}{E_0-H_0}\right]^m H'_{\rm hyp}\left[\frac{H'}{E_0-H_0}\right]^n\right|\Phi_0\right\rangle\ , \tag{9}$$

which is related to the hyperfine constant A_J as

$$A_J=\frac{1}{IJ}\left\langle\Psi_0\left|H'_{\rm hyp}\right|\Psi_0\right\rangle\ , \tag{10}$$

I referring to the nuclear spin and J to the magnitude of the total electronic angular momentum corresponding to Ψ_0.

The terms in the summation in Eq. (9) are referred to as (m,n) terms, with $(m+n)$ representing the order of the perturbation in H'. Each of these terms can be expressed [1(c)] in terms of diagrams. The rules for drawing those diagrams and the corresponding mathematical expressions for their evaluation, involving matrix elements of the perturbation Hamiltonian H' and the

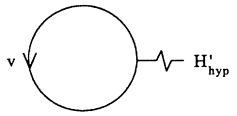

FIG. 1. (0,0) diagram. Direct valence contribution to the hyperfine field.

hyperfine operator $H'_{\rm hyp}$ over one-electron occupied and excited states and corresponding energy denominators, have been discussed in earlier literature [12] and will not be repeated here. The major contributors to the magnetic hyperfine constants in atomic systems are referred to [13,2(b)–2(d)] as direct or valence ECP and various orders of consistency and correlation effects. The corresponding diagrams making the most important contributions are shown in Figs. 1–6.

There are two important details of the procedure used in our investigation that we would like to mention here. These have to do with the departures from the point charge and point magnetic dipole moment approximations [13,14,2(b)–2(d)] for the nucleus. These departures are quite significant for moderately heavy atoms or ions such as Sr^+ and become increasingly important for even heavier systems. For incorporating the influence of the finite distribution of the nuclear charge, we have generated [1(c)3,2(b)–2(d)] the occupied and excited states using a spherical nuclear charge distribution with uniform density using a radius of the nucleus given by $1.2\times10^{-15}\,A^{1/3}$ m, A being the mass number of the nucleus. For incorporating the influence of the magnetic moment distribution, we have used appropriate correction factors for the nuclei of both Ca^+ and Sr^+ according to a prescription available in the literature [15] and used in earlier work [1(c),3,2(b)–2(d)].

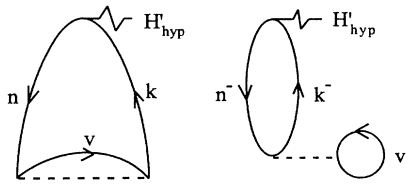

FIG. 2. Typical (0,1) diagrams. Diagrams representing (a) exchange core polarization and (b) phase-space contributions to the hyperfine field.

Before proceeding to the presentation of our results in Sec. III, we would like to state briefly here, for the sake of completeness, the relationship between the values of various diagrams and their contributions to the hyperfine constant A_J. For this purpose, we shall consider three diagrams that represent three important physical mechanisms for the origin of A_J. They are also the major contributors to A_J. Considering, for instance, the zeroth-order contribution from the valence electron represented by the diagram in Fig. 1 and the (0,0) term in the expansion in Eq. (9), the value of this diagram is given by [1(c),2(a)]

$$\Omega_{\rm val}=\int_0^\infty \frac{f_v g_v+g_v f_v}{r^2}dr=2\int_0^\infty \frac{f_v g_v}{r^2}dr=2\rho_v \qquad (11)$$

where f_v and g_v refer to the radial parts of the large and the small components of the one-electron wave function of the valence state, $4s_{1/2}$ for Ca^+ and $5s_{1/2}$ for Sr^+. For the ECP effect corresponding to diagram in Fig. 2(a), its contribution is given by

$$\Omega_{\rm ECP}=2\sum_k \left\{ \int_0^\infty \frac{f_{ns}g_{ks}+g_{ns}f_{ks}}{r^2}dr \frac{\int_0^\infty [f_{ns}(r_1)f_{vs}(r_2)+g_{ns}(r_1)g_{vs}(r_2)]\frac{1}{r_{12}}[f_{vs}(r_1)f_{ks}(r_2)+g_{vs}(r_1)g_{ks}(r_2)]dr_1dr_2}{\varepsilon_{ns}-\varepsilon_{ks}} \right\}$$
$$=2\rho_{\rm ECP}\,. \qquad (12)$$

In Eq. (12), f_{ns},g_{ns} and f_{ks},g_{ks} refer to the radial parts of the large and the small components of the one-electron relativistic core $ns_{1/2}$ states and excited $ks_{1/2}$ states, respectively, with ϵ_{ns} and ϵ_{ks} the corresponding relativistic one-electron energies. The factor 2 arises from the time-reversal symmetry associated with the diagram, namely, the equivalence of the (0,1) and the (1,0) terms in Eq. (9).

Finally, for the diagram in Fig. 4(a), the major second-order correlation diagram, its value is given by

$$\Omega_{\rm corr}=2a_{LJM}\sum_{k,k',k''} \left\{ \int_0^\infty \frac{f_{vs}g_{k''s}+g_{vs}f_{k''s}}{r^2}dr \right.$$
$$\times \frac{\int_0^\infty [f_{vs}(r_1)f_c(r_2)+g_{vs}(r_1)g_c(r_2)]\frac{1}{r_{12}}[f_k(r_1)f_{k'}(r_2)+g_k(r_1)g_{k'}(r_2)]dr_1dr_2}{(\varepsilon_{vs}-\varepsilon_{k''s})}$$
$$\left. \times \frac{\int_0^\infty [f_k(r_1)f_{k'}(r_2)+g_k(r_1)g_{k'}(r_2)]\frac{1}{r_{12}}[f_{k''s}(r_1)f_c(r_2)+g_{k''s}(r_1)g_c(r_2)]dr_1dr_2}{(\varepsilon_{vs}+\varepsilon_c-\varepsilon_k-\varepsilon_{k'})} \right\}$$
$$=2\rho_{\rm corr}\,, \qquad (13)$$

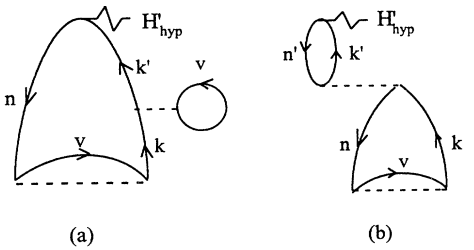

FIG. 3. Typical (0,1) diagrams. Diagrams representing (a) exclusion principle violation and (b) consistenecy contributions to the hyperfine field.

where c refers to the core states of the system under consideration, v refers to the s-valence state, and k,k', and k'' refer to the excited states. From the consideration of the nature of the hyperfine interaction and electron-electron vertices, it can be shown that k'' must have s symmetry while k and k' have the same L symmetry starting with $L=0$. The highest value we have considered is $L=4$, determined by examining the convergence with respect to L. In Eq. (13), as in Eq. (12), the factor of 2 arises from time-reversal symmetry [the equivalence of (0,2) and (2,0) terms in Eq. (9)]. The factor a_{LJM} arises from the angular integration associated with the two $1/r_{12}$ electron-electron vertices. Using Eq. (10), the corresponding contributions of these three diagrams to the hyperfine constant in megahertz can be written as

$$A_J(v)=\frac{K_J}{2\pi\alpha}\Omega_{\rm val}=\frac{K_J}{2\pi\alpha}2\rho_v\ , \tag{14}$$

$$A_J({\rm ECP})=\frac{K_J}{2\pi\alpha}\Omega_{\rm ECP}=\frac{K_J}{2\pi\alpha}2\rho_{\rm ECP}\ , \tag{15}$$

$$A_J({\rm corr})=\frac{K_J}{2\pi\alpha}\Omega_{\rm corr}=\frac{K_J}{2\pi\alpha}2\rho_{\rm corr}\ , \tag{16}$$

where

$$K_J=\frac{8\pi}{3}(\mu_B\mu_I/IJa_0^2h)\times10^{-6}\ , \tag{17}$$

in which μ_B and μ_I refer to the Bohr magneton and nuclear magnetic moment (in nuclear magneton), respectively, and α is the fine-structure constant.

In Eqs. (11)–(13), all quantities f,g, and ϵ are taken in atomic units. Therefore, the ρ_v, $\rho_{\rm ECP}$, and $\rho_{\rm corr}$ in Eqs. (14)–(16) will all have the same dimension (expressed in atomic units) corresponding to the radial integral in Eq.

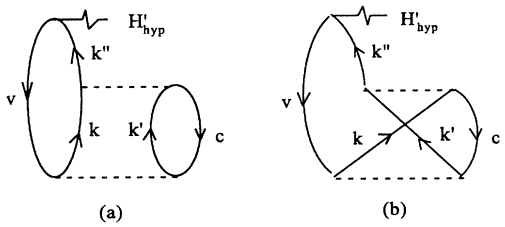

FIG. 4. Typical (0,2) diagrams. Diagrams representing second-order (a) direct and (b) exchange correlation contributions to the hyperfine field.

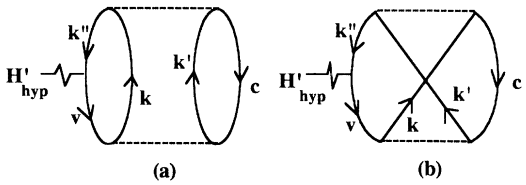

FIG. 5. Typical (1,1) diagrams. Diagrams representing second-order (a) direct and (b) exchange correlation contributions to the hyperfine field.

(11), since the rest of the terms in the summations in Eqs. (12) and (13) involve the ratio of two energy terms and are dimensionless. This statement applies to all the RLCMBPT diagrams including those in Figs. 1–6, all of which are evaluated in atomic units and then combined with the appropriate angular factors and the universal conversion factor $(K_J/2\pi\alpha)$ to get the results in frequency units (megahertz).

In comparing the hyperfine interactions in different related systems to analyze trends within the alkaline-earth-metal-ion series or between, for instance, the isoelectronic alkali-metal atoms and alkaline-earth-metal ions, it is more meaningful [6] to deal with the hyperfine field $H_{\rm hyp}$ instead of the hyperfine constant A_J. This is because the hyperfine field is independent of the nuclear moment and therefore reflects purely electronic properties. The relationship between $H_{\rm hyp}$ in tesla and A_J in megahertz is given by [6]

$$H_{\rm hyp}=\frac{IJh}{\mu_I}A_J\times10^{-6}\ . \tag{18}$$

III. RESULTS AND DISCUSSION: HYPERFINE INTERACTIONS IN Ca^+ AND Sr^+ IONS

We shall first present and discuss the results for the net hyperfine fields and contributions to them from various sources, in Ca^+ and Sr^+, and make comparisons with experimental results. This will be followed by a comparison in the trends of the contributions from different mechanisms in the alkaline-earth-metal-ion series with corresponding ones for alkali-metal atoms [6], noble-metal atoms [7], and singly charged group-IIB ions [8] isoelectronic with the latter.

Our results for the various contributions to the hyperfine fields in Ca^+ and Sr^+ are presented in Table I.

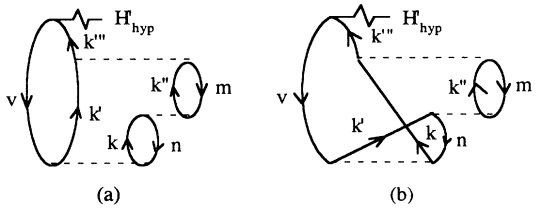

FIG. 6. Major third-order correlation diagrams. (0,3) diagrams representing (a) direct and (b) exchange correlation contributions to the hyperfine field.

TABLE I. Summary of contributions from different mechanisms to the hyperfine field H_{hyp} (in tesla) in $^{43}Ca^+$ and $^{87}Sr^+$ systems.

Mechanism	$^{43}Ca^+$	$^{87}Sr^+$
Valence	103.4	189.5
ECP	17.2	30.4
Phase space	1.6	3.2
EPV	−1.9	−3.6
Consistency	0.3	1.2
Net ECP	17.2	31.2
(0,2) correlation	14.7	51.4
(1,1) correlation	−0.4	−8.8
Total second-order correlation	14.3	42.6
Third-order correlation	1.0	3.0
Total	135.3±2.0	266.3±3.0
Experiment	138.99±0.17[a]	267.21±0.39[d]
	140.30±0.35[b]	
	142.39±2.61[c]	
Other theoretical calculations	142.7[e]	236.2[g]
	138.5[f]	

[a]Reference [3(a)].
[b]Reference [3(b)].
[c]Reference [3(c)].
[d]Reference [4].
[e]Reference [20].
[f]Reference [21].
[g]Reference [22]. Correlation effects are not included. The fields quoted are obtained by conversion from the published results (no error bars) in megahertz as explained in the text.

Also presented in this table are the hyperfine fields from experimental measurements, derived from the measured [3,4] hyperfine constants A_J using Eq. (18) with nuclear magnetic moments [16] of −1.317 26 and −1.093 603 nuclear magneton for the isotopes ^{43}Ca ($I=\frac{7}{2}$) and ^{87}Sr ($I=\frac{9}{2}$), respectively.

The first row in Table I presents the contribution from the (0,0) diagram in Fig. 1. This is the direct valence contribution [1(c)] from the 4*s* and the 5*s* states in Ca^+ and Sr^+, respectively, the leading effect in these ions and the only one that would have been present in the nonrelativistic restricted Hartree-Fock theory [17]. The trend of increasing direct contribution from Ca^+ to Sr^+, as has also been found for the isoelectronic alkali-metal atoms [6], is expected because of the increasing nuclear charge. The second row gives the ECP contribution [1(c)] represented by the diagram in Fig. 2(a). This effect is associated with the difference in the potentials experienced by the core-*s* electrons with opposite spins, due to the fact that the *s*-valence electron can have exchange interaction with only those *s*-core electrons with the same spin as itself. This is an effect that would be incorporated in the unrestricted Hartree-Fock procedure [18] and has also been studied in atomic and solid-state systems by perturbation methods [19]. The contributions to the ECP effect from individual core shells is given in Table II, which shows that the outermost *s*-core electron in both cases makes the leading contribution, due mainly to the stronger exchange interaction with the valence electron. The other *s*-core states make smaller but important contributions, the rate of decrease as one goes to the inner cores being significantly slower than in the isoelectronic alkali-metal atoms. In relativistic theory, the $p_{1/2}$ core electrons can also make nonvanishing ECP contributions [3,2(b)−2(d)], but from our experience in the heavier Ra^+ system, where such effects are expected to be as pronounced as they can be but found to be very small, one expects these contributions to be almost negligible in the present cases.

The third line of Table I gives the phase-space contribution [19], which is represented by the diagram in Fig. 2(b). This is associated with the difference generated by the fact that the valence state with down spin is empty and available for excitation from down-spin core states while the up-spin valence state is occupied (by the valence electron) and therefore not available for excitation from the up-spin core electrons. This effect is substantially smaller than the ECP effect because of the larger amount of available phase space (all the bound and continuum excited states) for excitations in the latter case. The next two rows of Table I present the contributions from the exclusion principle violation (EPV) diagram [13] in Fig. 3(a), which is associated with the use of the V^{N-1} potential, and the consistency effect [13]

TABLE II. Breakdown of contributions from the ECP effect to the hyperfine field in $^{43}Ca^+$ and $^{87}Sr^+$ (in tesla).

Contributing states	$^{43}Ca^+$	$^{87}Sr^+$
1*s*	2.9	2.4
2*s*	4.5	3.5
3*s*	9.8	6.7
4*s*		17.8
Total	17.2	30.4

represented by the diagrams in Fig. 3(b). These latter diagrams illustrate the influence of the self-consistent interaction between electrons. Thus, when a core state is perturbed through exchange with the valence state (leading to the ECP effect), its interaction with electrons in other states can cause changes in these latter states and consequently lead to additional contributions to the hyperfine field.

The contributions from these four mechanisms, i.e., ECP, phase space, EPV, and consistency, which are all one-electron effects owing their origin to the difference in the interaction between core states with different spin and the valence electron, are often combined and referred to as the net ECP contribution. This is listed in the sixth line of Table I. As in the case of direct effect, there is an increase in the net ECP contribution in going from Ca^+ to Sr^+. The dominant part of the net ECP contribution arises from the basic ECP effect of Fig. 2(a), as can be seen from Table I. Part of the reason for the increase in the ECP contribution in going from Ca^+ to Sr^+ is the larger number of core shells in Sr^+, as can be seen from Table II. However, in comparing the ECP contributions from individual core shells, it is meaningful to compare the outermost core shells, $3s$ and $4s$ in these two cases and correspondingly $2s$ and $3s$ and $1s$ and $2s$ for the more inner shells. For each of these pairs, the contribution for Sr^+ is always seen to be larger than that from the counterpart in Ca^+, the reason being the same as for the valence shell contributions (Table I), namely, the influence of the larger nuclear charge for Sr^+.

The correlation contributions to the hyperfine field are given in lines 7 and 8 in Table I. Among them, the second-order effects shown by the diagrams in Figs. 4 and 5 make the dominant contribution because correlation effect occurs for the first time in second order when one considers the electron-electron interactions in Eq. (9) (corresponding to the $m+n=2$ term in the perturbation expansion). Of the two types of second-order correlations, the contributions from (0,2) diagrams in Fig. 4 dominate over that of (1,1) represented by Fig. 5, a similar outcome as has been found in other alkaline-earth-metal ions [5] and other systems [6–8] with a single s-valence electron. The next line of Table I lists our estimates of the third-order correlation contribution to the hyperfine fields in Ca^+ and Sr^+. They are considered estimates because we have analyzed only a few third-order diagrams, some typical ones being shown in Fig. 6. These diagrams are chosen on the basis that they are related to the direct and exchange (0,2) diagrams, which made dominant contributions to the correlation effect in the second order. In Fig. 6, v refers to the valence electron, $4s$ for Ca^+ and $5s$ for Sr^+, while m and n refer to the outermost core electrons, $3s$ and $3p$ in Ca^+ and $4s$ and $4p$ in Sr^+. Again, these core electrons are selected because they are the major contributors in second-order correlations represented by Figs. 4 and 5. The net values of the hyperfine fields obtained by our calculation are given in line 10 of Table I. The confidence limits placed on these results were obtained through a consideration of fourth- and higher-order contributions and computational accuracy.

Following our net calculated hyperfine fields, Table I lists the experimental results for the two ions. These data were available as hyperfine constants A_J in megahertz and have been converted to the hyperfine fields $H_{\rm hyp}$ in tesla by applying Eq. (18), using the nuclear magnetic moments [16] of ^{43}Ca and ^{87}Sr stated earlier in this section. Only one result of A_J is available [4] for $^{87}Sr^+$ in the literature. On the other hand, there are three available experimental values [3] of the hyperfine constant A_J for the $^{43}Ca^+$ ion, all of which have been converted and listed after our theoretical result in Table I.

The hyperfine fields obtained from the other theoretical investigations are listed at the end of Table I for comparison with our results. These fields are obtained from the published results for the hyperfine constants in Refs. [20–22] using the conversion factor in Eq. (18). For Sr^+, our calculated value is in excellent agreement with the experimental result. For Ca^+, our result is within 1.5–2.0 % of the experimental values from the two most recent measurements. This very good agreement in both cases is typical of the earlier calculations of hyperfine field in other alkaline-earth-metal ions [5] and alkali-metal atoms [6] using the same RLCMBPT technique [1,2].

As regards other theoretical calculations for $^{43}Ca^+$, two results [20,21] have been reported in the literature as shown in Table I. Both of them use a differential equation approach to study the perturbation effects due to the hyperfine interaction [19] and electron-electron interaction [20] instead of the summations over excited states used in our procedure. The earlier [20] value obtained using this differential equation approach is 142.7 T and the more recent one [21] is 138.5 T. The published hyperfine constants by this procedure were given in MHz as 819 and 794.7 MHz, respectively [20,21]. They have been converted to Tesla by applying the conversion factors mentioned in Sec. II. These values are to be compared with our fully RLCMBPT results of 135.3 T (776.3 MHz). The procedure [20,21] used for the earlier results is very different from ours and also has a number of other differences as discussed in detail in an earlier paper [13] on Ra^+ by our group. Among them are the use of Ca^{2+} wave functions as a starting point instead of the Hartree-Fock wave functions we have adopted, the use of a scale factor to the calculated nonrelativistic correlation contribution to incorporate relativistic effects, and a partitioning of ECP and correlation contributions different from those obtained by the composites of different physical effects represented by our diagrams. In spite of these differences in approaches, the numerical agreement between the earlier results and ours is rather good as in the case [13] of Ra^+. However, because of the differences in approaches, it is not possible to compare contributions from individual mechanisms such as valence, ECP, and correlation in the two cases.

For Sr^+, the earlier published result [22] using the differential equation approach did not include correlation effects and the net result there including valence and ECP effects is found to be 236.2 T after converting from their hyperfine constant of 875 MHz using the same procedure

just mentioned for the Ca^+ case. Considering that our RLCMBPT result of 266.3 T, which does include correlation effects, is in excellent agreement with the experimental value of 267.2 T, it would be interesting to see whether the treatment of correlation effects in the differential equation approach [22] could bridge the gap between their net result from valence and ECP effects and the experimental result.

IV. DISCUSSIONS OF TRENDS OF CONTRIBUTIONS TO THE HYPERFINE FIELDS FROM VARIOUS PHYSICAL MECHANISMS IN ALKALINE-EARTH-METAL IONS AND RELATED SYSTEMS

We consider next the trends in the contributions from the net ECP and correlation effects to the hyperfine fields in the alkaline-earth-metal ions and compare them with those from other systems with a single *s*-valence electron, namely, the alkali-metal [6] and noble-metal [7] atoms and singly charged group-IIB ions [8] Zn^+, Cd^+, and Hg^+. As mentioned in earlier work [6] on the trends in the alkali-metal-atom series, it is most meaningful to consider the ratios H_{ECP}/H_{val} and H_{corr}/H_{val} in the discussion. Using these ratios allows one to focus on the influence of electron-electron interactions of the exchange and the correlation types involving the valence and primarily the outer core electrons. The expected monotonic increase in the valence and the core electron densities at the nuclear sites associated with the hyperfine vertex in the various diagrams is effectively filtered out by taking these ratios.

The variations in H_{ECP}/H_{val} over the alkaline-earth-metal-ion, alkali-metal-atom, noble-metal-atom, and group-IIB-ion series are presented in Fig. 7. The corresponding variations in H_{corr}/H_{val} of the alkaline-earth-metal-ion and alkali-metal-atom series are shown in Fig. 8 and those of the noble-metal-atom and group-IIB-ion series are given in Fig. 9. In presenting our results in these figures, for the sake of display, we have utilized the ionic radii of the single positively charged alkali-metal

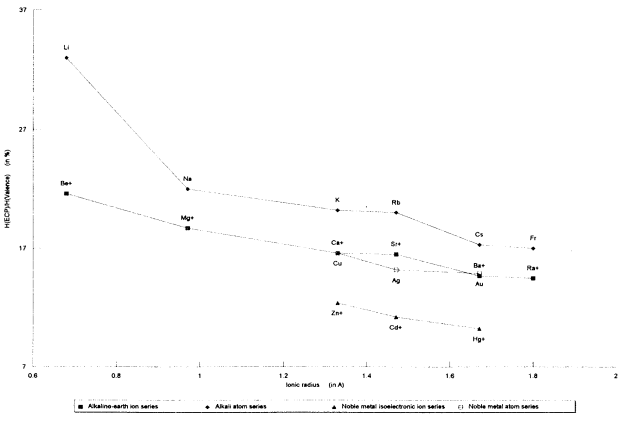

FIG. 7. Exchange core polarization (ECP) contributions to the hyperfine field in the alkaline-earth-metal-ion, alkali-metal-atom, group-IIB-ion and noble-metal-atom series, as fractions of valence contributions. Ionic radii used frefer to the positive alkali-metal ions, as explained in the text.

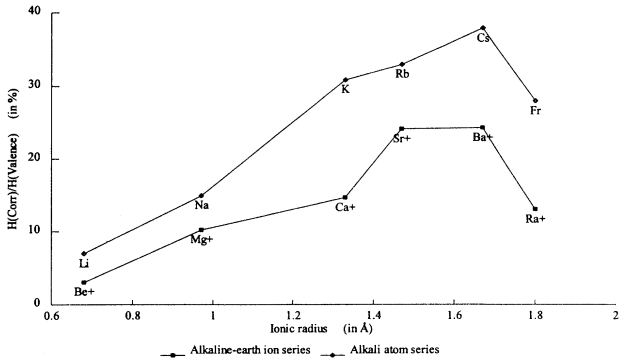

FIG. 8. Many-body correlation contribution to the hyperfine field in the alkaline-earth-metal-ion and alkali-metal-atom series, as fractions of valence contributions. Ionic radii used refer to the positive alkali-metal ions, as explained in the text.

ions as the reference points for the various members of each series. All systems with similar valence electrons are placed on the same reference radius for purposes of appropriate comparison. An example of this choice is for instance the pair of ions Ca^+ and Zn^+, both of which have a 4*s* valence electron and are placed at the ionic radius of K^+ for suitable comparisons in Fig. 7. The same is also true for K and Ca^+ (both placed at the K^+ ionic radius) in Fig. 8 and for Cu and Zn^+ (both placed at the K^+ ionic radius) in Fig. 9.

Since one cannot make measurements of the individual contributions to the hyperfine fields, it is not possible to verify the theoretical predictions for the latter, such as the direct, the ECP, and the correlation contributions. However, as pointed out in the Introduction, the good agreement between theory and experiment for the total hyperfine fields strongly suggests that the calculated results for the individual contributions should be quite accurate and hence also the trends in H_{ECP}/H_{val} and H_{corr}/H_{val}. A list of the total hyperfine fields [23], both experimental and theoretical, as well as individual contributions for all the four series under consideration here, is presented in Tables III–VI for ready reference. Also included in these tables are the ratios of H_{ECP}/H_{val} and H_{corr}/H_{val}, which are plotted in Figs. 7–9.

Focusing on Fig. 7, the trend of H_{ECP}/H_{val} in the

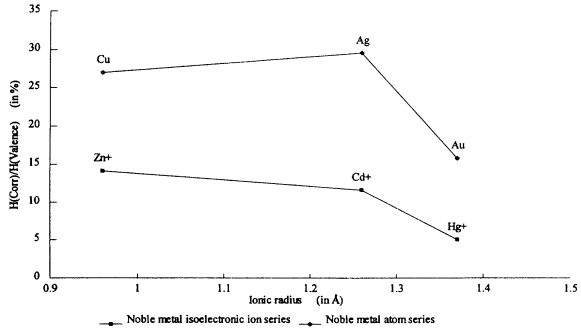

FIG. 9. Many-body correlation contribution to the hyperfine field in the group-IIB-ion and noble-metal-atom series. Ionic radii used refer to the appropriate positive alkali-metal ions, as explained in the text.

TABLE III. Values of ECP and many-body correlation contributions to the hyperfine fields in the alkaline-earth-metal ion series. The values of the contributions to the hyperfine fields are expressed in tesla.

System	H_{val}	H_{ECP}	H_{corr}	H_{ECP}/H_{val} (%)	H_{corr}/H_{val} (%)	H_{total}[a]	H_{expt}[a]
Be^+	41.7	9.0	1.3	21.6	3.1	52.0	52.2
Mg^+	89.4	16.7	9.2	18.7	10.3	115.3	114.3
Ca^+	103.4	17.2	15.3	16.6	14.7	135.3	139.0
Sr^+	189.5	31.2	45.6	16.5	24.1	266.3	267.2
Ba^+	315.4	46.5	76.5	14.7	24.3	438.4	422.8
Ra^+	971.0	141.0	127.0	14.5	13.1	1239.0	1226.0

[a]For theoretical and experimental results of Be^+, see Ref. [24]; for Mg^+, see Ref. [5(a)]; for Ba^+, see Ref. [5(b)]; for Ra^+, see Ref. [13]; for experimental results of Ca^+ and Sr^+, see Refs. [3(a)] and [4], respectively.

alkaline-earth-metal ion series and comparing with the other three series, we notice the following features.

(i) The trend of decrease in H_{ECP}/H_{val} going from the lightest ion Be^+ to the heaviest Ra^+ is very similar to that of the isoelectronic neutral alkali-metal-atom series.

(ii) The value of H_{ECP}/H_{val} for each alkaline-earth-metal ion is significantly smaller than that of the corresponding isoelectronic alkali-metal atom.

(iii) The decrease in H_{ECP}/H_{val} from Be^+ to Mg^+ is somewhat more significant than the decrease in going through the rest of the series. However, this drop is much less dramatic than the decrease from Li to Na.

(iv) The alkaline-earth-metal-ion H_{ECP}/H_{val} results are significantly higher than those for the corresponding group-IIB ions. The trend of decrease over the two series is, however, somewhat different, the variations over the alkaline-earth-metal-ion series being more pronounced.

(v) The values of H_{ECP}/H_{val} for the neutral noble-metal atoms are comparable to those for the corresponding neutral alkali-metal-atom series. Also, the neutral noble-metal-atom results are substantially higher than those of the isoelectronic group-IIB ions, a feature similar to that pointed out in (ii).

It is worthwhile to attempt to understand the reasons that lead to the listed main features of the trends in H_{ECP}/H_{val} obtained from Fig. 7 since they could provide valuable insights into the physical factors involved. The first feature of similar overall decrease of H_{HCP}/H_{val} in the alkaline-earth-metal-ion and alkali-metal-atom series is understandable because both classes of systems are very similar, with single s-valence electron and p and s outermost cores. The second feature of smaller values of H_{ECP}/H_{val} for the alkaline-earth ions as compared to their counterparts in alkali-metal-atom series is expected to be a consequence of the tighter binding of the core electrons in the ions. This makes the core electrons less deformable than those in the alkali-metal atoms under the influence of the exchange potential due to the valence electron.

Considering the third feature, the rapid decrease of H_{ECP}/H_{val} in going from Li to Na, it had been explained in earlier work [6] as a result of the presence of the $2p$ core in Na, which has a shielding effect on the $2s$ core. Since the exchange interaction between the $2s$-core and the $3s$-valence electron is the major contributor to the ECP effect, this shielding factor would cause substantial decrease in ECP as compared to the case of Li, where such a factor is absent. The corresponding weaker decrease in H_{ECP}/H_{val} from Be^+ to Mg^+ is most likely a consequence of the positive charge on these ions that pulls the valence electron inwards, lessening the importance of the shielding effect of the $2p$-core electrons. The fourth feature of considerably weaker H_{ECP}/H_{val} in the group-IIB-ion series as compared to the alkaline-earth-metal-ion series could be the result of two factors. The first is that the presence of the outermost d core in group-IIB ions increases the shielding effect on the exchange interaction between the s-valence electron and the

TABLE IV. Values of ECP and many-body correlation contributions to the hyperfine fields in the alkali-metal atom series. The values of the contributions to the hyperfine fields are expressed in tesla.

System	H_{val}	H_{ECP}	H_{corr}	H_{ECP}/H_{val} (%)	H_{corr}/H_{val} (%)	H_{total}[a]	H_{expt}[a]
Li	8.6	2.8	0.6	33.0	7.0	12.0	12.1
Na	27.9	6.1	4.2	22.0	15.0	38.5	39.3
K	37.6	7.6	11.6	20.2	30.9	56.8	58.0
Rb	80.7	16.1	26.6	20.0	33.0	123.2	122.2
Cs	134.0	23.2	50.9	17.3	38.0	208.6	205.5
Fr	453.0	77.0	126.8	17.0	28.0	656.8	660.0

[a]See Ref. [6] for references to the theoretical and the experimental results, except for H_{expt} of Fr, which is based on the observed hyperfine constant in ^{213}Fr [25] and the measured ^{211}Fr magnetic moment of 3.996(77) nuclear magnetons [26].

TABLE V. Values of ECP and many-body correlation contributions to the hyperfine fields in the group-IIB-ion series. The values of the contributions to the hyperfine fields are expressed in tesla.

System	H_{val}	H_{ECP}	H_{corr}	H_{ECP}/H_{val} (%)	H_{corr}/H_{val} (%)	H_{total}[a]	H_{expt}[a]
Zn^+	353.5	43.8	50.3	12.4	14.2	447.6	
Cd^+	647.5	72.4	75.6	11.2	11.7	795.5	826.1
Hg^+	2291.5	234.3	116.4	10.2	5.1	2642.2	2626.1

[a]See Ref. [8] for references to the theoretical and the experimental results.

outermost *s* cores, thus reducing the strength of the ECP effect relative to that in the corresponding alkaline-earth-metal ions. The second possible source could be the weaker shielding effect on the nuclear charge by the *d*-core electrons, making the outermost *s* core more tightly bound relative to the corresponding ions in alkaline-earth-metal series, thus leading to a weaker ECP effect.

Finally, the fifth observed character of the trends involving weaker H_{ECP}/H_{val} of the noble-metal atoms compared to that of the alkali-metal atoms can be understood by the same reasoning given earlier for the similar trend between the group-IIB-ion and the alkaline-earth-metal-ion series. In addition, the relatively larger H_{ECP}/H_{val} for the neutral noble-metal atoms as compared to the group-IIB ions can also be understood by the influence of the extra positive charge of the latter, an argument [1(c)] similar to the one used earlier in explaining the second observed feature of the trends.

The many-body correlation contributions, presented by the calculated ratios of H_{corr}/H_{val} in Tables III–VI and graphically in Figs. 8 and 9, indicate the following trends.

(i) The variation of H_{corr}/H_{val} in going from the lightest ion Be^+ to the heaviest Ra^+ is seen to follow the same overall trend as that of the neutral alkali-metal atoms, with an increase up to Ba^+ (Cs) followed by a significant drop in going to Ra^+ (Fr). This feature is different from that of the ECP effect in Fig. 7, where there is a continuous decline in H_{ECP}/H_{val}.

(ii) There is, however, a difference in detail between the trend in the alkaline-earth-metal-ion and the alkali-metal-atom series. The nearly flat behavior of the H_{corr}/H_{val} curve in Fig. 8 between Sr^+ and Ba^+ before the sharp descent to Ra^+ is in marked contrast to the significant rise from Rb to Cs. Further, as in the case of the H_{ECP}/H_{val} trend in Fig. 7, the H_{corr}/H_{val} curve for the alkaline-earth-metal ions is lower than the corresponding one for the neutral alkali-metal-atom series.

(iii) The trend in the group-IIB ions from Zn^+ to Hg^+ in Fig. 9 is very similar to that in the alkaline-earth-metal ions starting from Sr^+ in Fig. 8. There is a slight decrease in going from Zn^+ to Cd^+ followed by a substantial decrease in going to Hg^+, mirroring quite closely the change from Sr^+ through Ba^+ to Ra^+, the only difference being the near constancy of H_{corr}/H_{val} from Sr^+ to Ba^+. Correspondingly, the trend of the neutral noble-metal-atom series resembles that of the alkali-metal atoms, the slight difference being the slower increase in H_{corr}/H_{val} from Cu to Ag in contrast to the sharper increase from Rb to Cs.

(iv) As in the case of H_{ECP}/H_{val}, the magnitudes of the H_{corr}/H_{val} ratios for the alkaline-earth-metal ions as seen from Figs. 8 and 9 are significantly larger than the corresponding ones for the group-IIB ions. The same observation applies to the relative trends between the noble-metal-atom and the alkali-metal-atom series.

Similar to the case of the observed tends in H_{ECP}/H_{val}, we will attempt to understand the features just listed for the trends in H_{corr}/H_{val}. Considering the first of these, the trend of the alkaline-earth-metal ions can be explained by the same arguments as proposed in the literature [6] for alkali-metal atoms. This has to do with the fact that the main correlation diagrams in Figs. 4 and 5 can be considered as representing the contribution from a Van der Waals (VDW) type of interaction between the outermost core electrons and the valence electron. The VDW type of effect involves a mutual polarization of the core and the valence electrons that depends on both their deformabilities and the relative separation between them. These two factors are competitive because the increasing deformabilities would lead to an increase in the correlation effect, while the separation factor would cause a decrease. It appears from Fig. 8 that the deformability effect dominates between Li and Cs and is superseded by the separation factor in going from Cs to Fr. The same considerations would also explain the increase in H_{corr}/H_{val} from Be^+ to Ba^+ and the rapid drop from Ba^+ to Ra^+. The relative difference in trends in going from Sr^+ to Ba^+ as compared to that from Rb to Cs,

TABLE VI. Values of ECP and many-body correlation contributions to the hyperfine fields in the noble-metal-atom series. The values of the contributions to the hyperfine fields are expressed in tesla.

System	H_{val}	H_{ECP}	H_{corr}	H_{ECP}/H_{val} (%)	H_{corr}/H_{val} (%)	H_{total}[a]	H_{expt}[a]
Cu	178.1	29.5	48.1	16.6	27.0	255.7	260.0
Ag	366.3	55.7	108.5	15.2	29.6	530.5	499.1
Au	1527.3	227.3	242.7	14.9	15.9	1997.3	2074.5

[a]See Ref. [7] for references to the theoretical and the experimental results.

which we noted in the second feature from Fig. 8, could be the result of a different degree of competition between the two factors in the alkaline-earth-metal-ion and alkali-metal-atom series. As regards the weaker correlation effect in the alkaline-earth-metal ions compared to that in the alkali-metal atoms, this trend would be expected because of the lesser deformabilities in the latter series.

Concerning the third feature in the trend, namely, the slow variation from Zn^+ to Cd^+ and a more rapid decrease from Cd^+ to Hg^+, it seems that at the beginning of the series, the separation factor is comparable in effect to the competing deformability factor and then dominates in going to the heaviest ion Hg^+. The same arguments could be used to explain the trend over the noble-metal-atom series. This feature is similar to that for the alkaline-earth-metal ions starting with Sr^+ and a little different from that for the alkali-metal atoms, which are seen from Fig. 9 to show a significant increase from Rb to Cs followed by a drop in going to Fr.

Regarding the fourth feature, a weaker correlation effect for group-IIB ions compared to that for alkaline-earth-metal ions, one again has to consider the relative changes in deformabilities of the valence and outermost cores as well as the relative separations between the two. As discussed earlier for the trends in the ECP contributions, the primary cause was expected to be the result of the diffusiveness of the outermost d orbitals, which would lead to weaker shielding of the nuclear potential. This in turn could make the other cores more tightly bound, explaining the weaker ECP effect for the group-IIB ions. However, the same weaker shielding effect due to the d core would make the s-valence electron more tightly bound. In the present case of correlation effects where the deformabilities of both the d-core and the s-valence electron are involved, one expects the deformabilities of the relatively diffuse d-core orbitals in the group-IIB ions to be stronger than that of the p-core orbitals in the corresponding alkaline-earth-metal ions. On the other hand, the tighter valence electron for the group-IIB ions would be expected to have lesser deformability than that of the alkaline-earth-metal ions. The observed trends in the correlation effects in these two cases then suggests that the lesser deformability of the valence electron in the group-IIB systems is the determining factor. The same argument can also be applied to explain the weaker correlation effect for the noble-metal atoms as compared to the alkali-metal atoms. This argument is based on the assumption that the separation factor is not an important element, which is likely to be correct since one is comparing systems with similar valence electrons and sizes. Thus it appears that the observed trends in ECP and correlation effects over each of the four series, and the relative trends between them, can be reasonably well understood from a physical point of view by considering the changes in deformabilities of the orbitals involved and the separations between the valence and the pertinent core orbitals.

V. CONCLUSION

The first-principle relativistic linked-cluster many-body perturbation theory applied to the hyperfine structure in the ^2S ground state of Ca^+ and Sr^+ in the present work has produced very good agreement with the experimental results. The calculations on both these systems enable us to study the trends in the relative contributions from the two leading mechanisms for the hyperfine interaction, namely, exchange core polarization and many-body correlation effects, throughout the entire alkaline-earth-metal-ion series.

With the completion of this work, we now have results available concerning hyperfine fields in all the four related important series characterized by a single s-valence electron outside closed shells (alkaline-earth-metal ions, alkali-metal atoms, isoelectronic group-IIB ions, and noble-metal atoms), all obtained through the same first-principle RLCMBPT procedure [1,2]. The availability of these results allows us to study not only the important features in each individual series, but also the relative trends between any two of them. This provides us with an opportunity to understand, at the individual mechanism level, the nature of the hyperfine interactions in atomic and ionic systems and obtain insights into such factors as the deformabilities of core and valence electrons, the effective charges on the systems, the relative separations between the core and the valence electrons, and the consequences of relative changes in these factors on the systems in the corresponding series. Considering all these factors, we have been able to analyze and explain in a satisfactory manner the physical reasons involved in the observed trends in connection with the ECP and correlation effects, which should enhance our overall understanding of the nature of these important mechanisms for the hyperfine interaction. In addition, the good agreement with experimental data for all these systems increases our confidence in the relativistic linked-cluster many-body perturbation theoretic method used to calculate the hyperfine properties in atomic and ionic systems.

[1] (a) J. Andriessen, K. Raghunathan, S. N. Ray, and T. P. Das, Phys. Rev. B **15**, 2533 (1977); (b) J. Andriessen, D. Van Ormondt, S. N. Ray, and T. P. Das, J. Phys. B **11**, 2601 (1978); (c) T. P. Das, Hyp. Int. **34**, 149 (1987).

[2] (a) Mina Vajed-Samii, S. N. Ray, T. P. Das, and J. Andriessen, Phys. Rev. A **20**, 1787 (1979); (b) Mina Vajed-Samii, J. Andriessen, B. P. Das, S. N. Ray, T. Lee, and T. P. Das, Phys. Rev. Lett. **48**, 133 (1982); (c) **49**, 1466 (1982); (d) **49**, 1800 (1982).

[3] (a) A. T. Goble and S. Maleki, Phys. Rev. A **42**, 649 (1990); (b) E. Silverans, L. Vermeeren, R. Neugart, P. Lievens, and the ISOLDE Collaboration, Z. Phys. D **18**, 351 (1991); (c) F. M. Kelly, H. Kuhn, and A. Pery, Proc. Phys. Soc. London Sect. A **67**, 450 (1954).

[4] R. Beigang, W. Makat, A. Timmermann, and P. J. West, Phys. Rev. Lett. **51**, 771 (1983).

[5] (a) S. Ahmad, J. Andriessen, and T. P. Das, Phys. Rev. A **27**, 2790 (1983); (b) S. Ahmad, J. Andriessen, K. Raghunathan, and T. P. Das, *ibid.* **25**, 2923 (1982).
[6] Mina Vajed-Samii, J. Andriessen, B. P. Das, S. N. Ray, Tauesul Lee, and T. P. Das, J. Phys. B **15**, L379 (1982).
[7] R. W. Dougherty, Surya N. Panigrahy, and T. P. Das, Phys. Rev. A **47**, 2710 (1993).
[8] Surya N. Panigrahy, R. W. Dougherty, and T. P. Das, Phys. Rev. A **44**, 121 (1991).
[9] T. P. Das, *Relativistic Quantum Mechanics of Electrons* (Harper & Row, New York, 1973), Chap. 7.
[10] James E. Rodgers, Ribha Roy, and T. P. Das, Phys. Rev. A **14**, 543 (1976).
[11] K. A. Brueckner, Phys. Rev. **100**, 36 (1956); J. Goldstone, Proc. R. Soc. London Ser. A **239**, 267 (1957).
[12] Edward S. Chang, Robert T. Pu, and T. P. Das, Phys. Rev. **174**, 1 (1968).
[13] Surya N. Panigrahy, R. W. Dougherty, S. Ahmad, K. C. Mishra, T. P. Das, J. Andriessen, R. Neugart, E. W. Otten, and K. Wendt, Phys. Rev. A **43**, 2215 (1991).
[14] V. A. Dzuba, V. V. Flambaum, and O. P. Sushkov, Phys. Scr. **32**, 507 (1985).
[15] H. Kopfermann, *Nuclear Moments* (Academic, New York, 1958), p. 123.
[16] Pramila Raghavan, At. Data Nucl. Data Tables **42**, 210 (1989); **42**, 223 (1989).
[17] D. R. Hartree, *The Calculation of Atomic Structures* (Wiley, New York, 1957).
[18] R. E. Watson and A. J. Freeman, Phys. Rev. **123**, 2027 (1961); N. Bessis, H. Lefebvre-Brion, C. M. Moser, A. J. Freeman, R. K. Nesbet, and R. E. Watson, *ibid.* **135**, A588 (1964).
[19] M. H. Cohen, D. A. Goodings, and V. Heine, Proc. Phys. Soc. London **73**, 811 (1959); G. D. Gaspari, Wei-Mei Shyu, and T. P. Das, Phys. Rev. **134**, A960 (1964); Wei-Mei Shyu, G. D. Gaspari, S. D. Mahanti, L. Tterlikkis, and T. P. Das, in *Magnetic Resonance,* edited by C. K. Coogan, N. S. Ham, S. N. Stuart, J. R. Pilbrow, and G. V. H. Wilson (Plenum, New York, 1970).
[20] Ann-Marie Mårtensson-Pendrill and Sten Salomonson, Phys. Rev. A **30**, 712 (1984).
[21] Ann-Marie Mårtensson-Pendrill, Anders Ynnerman, Håkan Warston, Ludo Vermeeren, Roger E. Silverans, Alexander Klein, Rainer Neugart, and Christoph Schulz, Peter Lievens, and the ISOLDE Collaboration, Phys. Rev. A **45**, 4675 (1992).
[22] J.-L. Heully and A.-M. Mårtensson-Pendrill, Phys. Scr. **31**, 169 (1984).
[23] See Refs. [6–8] for the theoretical results of the total hyperfine constants of the individual members of the alkali-metal-atom, noble-metal-atom, and group-IIB-ion series and the references to the experimental measurements therein.
[24] Surya Panigrahy, R. W. Dougherty, and J. Andriessen, Phys. Rev. A **40**, 1765 (1989).
[25] S. Lieberman *et al.*, Phys. Rev. A **22**, 2732 (1980).
[26] C. Ekström and L. Robertsson, in *Proceedings of the Eighth International Conference on Atomic Physics (ICAP-8), Göteberg, Sweden, 1982,* edited by I. Lundgren, A. Rosén, and S. Svanberg (Plenum, New York, 1983).